LAWRENCE
LIVERMORE
NATIONAL
LABORATORY

LLNL-JRNL-480181

THERMODYNAMIC ASSESSMENT OF THE AM-PU SYTEM WITH INPUT FROM AB INITIO

P. E. A. Turchi, A. I. Landa, P. A. Soderlind

April 12, 2011

Journal of Nuclear Materials

Disclaimer

submitted to Journal of Nuclear Materials

Thermodynamic assessment of the Am-Pu system with input from ab initio

P. E. A. Turchi[a,*], A. I. Landa[a], and P. A. Söderlind[a]

[a]*Lawrence Livermore National Laboratory (L-352), P.O. Box 808, Livermore, California 94551, USA*

(April 6, 2011)

Abstract

Based on the CALPHAD approach, thermodynamic properties and phase diagram of the Am-Pu system are assessed with input from results of *ab initio* electronic-structure calculations within the framework of density-functional theory. Despite the limited availability of experimental data on this binary system, thermodynamic assessment has been performed and two phase diagrams are proposed that make distinction at high temperature between the relative stability of the bcc phase and the liquid state. Our investigation provides guidance and motivates further experimental studies.

Keywords: nuclear reactor materials, first-principles, thermodynamics, phase diagrams

I. INTRODUCTION

With the current interest in Gen-IV advanced nuclear reactors [1] and a better management of actinide-based fuels, and in the disposition of transuranic elements (TRU), there is a need to better understand the thermodynamic properties of mixtures of actinide elements. In particular, since the amount of Am in Pu in the next generation of actinide burner reactors may be significant, it becomes increasingly important to include Am in a thermodynamic database dedicated to nuclear fuel materials to understand its impact on the stability properties of Pu-based alloys. Actually, americium 241 appears as a decay product of the 241 isotope of Pu with a significant rate in wt.% Am/30 days of 5.477 10^{-3} wt. % ^{241}Pu.

The assessed phase diagram of Am-Pu reported in Refs. [2–4] reproduced in Fig. 1a is primarily based on the work of Ellinger *et al.* [5] that used micrographic and X-ray diffraction methods. It should be noted that at the time the phase diagram of Am-Pu was explored experimentally, with a focus mostly on the Pu-rich region of the phase diagram, only two allotropes of Am were known. This explains why the proposed phase diagram shown in Fig. 1a is incomplete, especially in the high-temperature solid-phase portion. Phase-diagram results have recently been updated by Shushakov *et al.* [6] with a combination of high-temperature X-ray diffraction analysis, differential thermal and microstructural analysis, and hydrostatic determination of density. That work accounts for more complete data on the polymorphism of metallic americium [7,8] as shown in Fig. 1b. Namely, as a function of temperature, Am exhibits three allotropes; double hexagonal close-packed (dhcp) that is the ground state, then face-centered cubic(fcc), and body-centered cubic (bcc), before melting according to: α-Am (dhcp) $\rightarrow$ β-Am (fcc) $\rightarrow$ γ-Am (bcc) $\rightarrow$ Liquid, with transition temperatures of 745, 1056, and 1176 °C, respectively. One salient difference between the "American" and "Russian" versions of the Am-Pu phase diagram regards the bcc solid solution. In the "American" version, Fig. 1a, there is a peritectic reaction at about 665 °C: Liquid + $\delta \rightleftharpoons \epsilon$ at the Pu edge of the phase diagram with a limited solubility of about 8 at.%

Am in the bcc phase of Pu. On the contrary, the "Russian" version of the phase diagram in Fig. 1b shows the bcc phase extended in the entire range of alloy composition. Both phase diagrams agree on the existence of a continuous series of fcc-based solid solutions that form between δ-Pu and β-Am at high temperatures, with a solubility range of 20 to 93.9 at.% Pu at room temperature, and so far no evidence of ordering or clustering phenomena on the fcc lattice at low temperatures. Because of the propensity of fcc-based Am-Pu alloys to display substantial undercooling, no two-phase region between α-Am and δ-Pu was observed experimentally, see Fig. 1. Instead, on the Am rich-side of the phase diagram, a single-phase structure made of four-layer dense packing of hexagonal layers (ABAC, dhcp) was identified with a gradual transformation to a three-layer fcc structure (ABC) at elevated temperature. This absence of a two-phase region could be attributed to slow kinetics or to a narrow equilibrium two-phase field that would be difficult to observe. In addition, the high volatility of Am, as mentioned in Ref. [5], makes sample preparation itself and subsequent control of alloy composition very challenging.

Despite recent progress in modeling electronic structure and energetics of pure plutonium [9–12] an accurate determination of the electron correlation effects in Pu and its alloys still remains challenging [13]. Unfortunately, dynamical-mean-field theory is currently unable to model phase stability and energetics in spite of being able to produce realistic spectra for δ-Pu [14,15]. The situation becomes even more difficult when considering the Am-Pu system since Am is known to exhibit all the characteristics of $5f$ localization behaving in its ground state as the rare-earth elements. In contrast, for Pu the $5f$ electrons are delocalized albeit very close to the borderline between the two behaviors. One should also remember that changes in volume (pressure) and perhaps alloying changes the electronic structure in Am to become more like that of Pu [16]. From this standpoint, the Am-Pu system is indeed an interesting system to thoroughly study both experimentally and theoretically.

A debate is still going on [17] regarding the correctness of state-of-the-art density-functional theory (DFT) to properly treat the electronic structure of Am [16,18] and Pu systems. However, recent DFT results [19,20] have encouraged us to select this methodol-

ogy to generate crucial energetic data on heats of formation versus composition that were then used to assess the thermodynamic properties of Am-Pu in the whole range of composition and temperature. To do so, we considered the CALPHAD (CALculations of Phase Diagrams) methodology that has been since the 70's very successful in describing alloy thermodynamics of complex multi-component alloys [21–23].

Hence, statics of phase transformations in this alloy system has been modeled with a scheme that couples assessed thermo-chemical data of the endpoints, Am and Pu, and phase boundary information from experimentally determined phase diagram, together with input from *ab initio* calculated energetics to the thermodynamic database, all in the framework of the CALPHAD approach. This procedure will allow us to provide (i) some insight on the Am-Pu phase diagram; (ii) an explanation to the main difference between the two versions of the phase diagram; and (iii) offer guidance for subsequent experimental work in regions of temperature and composition where thermodynamic data validation is needed the most.

The paper is organized as follows. In Sec. II we briefly describe the thermodynamic modeling based on the CALPHAD methodology, and take this opportunity to summarize the results of Am-Pu phase diagram assessment by Ogawa based on the Brewer valence bond model [24], and most recently by Kurata by using a phenomenological CALPHAD approach [25]. In Sec. III, we present the computational details of the *ab initio* theoretical techniques together with the results on equilibrium properties, electronic structure, and energetics for the Am-Pu system. In Sec. IV, phase diagram assessment based on input from *ab initio* results and experimental information is presented. Finally, in Sec. V, we provide guidance for future experimental work together with some concluding remarks.

II. THERMODYNAMIC MODELING

In the CALPHAD approach, the Gibbs energy of individual phases is modeled, and the model parameters are collected in a thermodynamic database. It is the modeling of the Gibbs energy of individual phases and the coupling of phase diagram and thermo-

chemistry that make CALPHAD a powerful technique in computational thermodynamics of multi-component materials. For the two unaries (X=Am, Pu) the Gibbs energy function ${}^0G^{\phi}_{\rm X}(T) = G^{\phi}_{\rm X}(T) - H^{\rm SER}_{\rm X}$ for the element X in the phase ϕ (ϕ = liquid, bcc (ϵ-Pu, γ-Am), α-Am, α-Pu, β-Pu, γ-Pu, fcc (δ-Pu, β-Am), and δ'-Pu) is written in the most general form as

$$ {}^0G^{\phi}_{\rm X} = a^{\phi}_{\rm X} + b^{\phi}_{\rm X}T + c^{\phi}_{\rm X}TlnT + d^{\phi}_{\rm X}T^2 + e^{\phi}_{\rm X}T^{-1} + f^{\phi}_{\rm X}T^3 + g^{\phi}_{\rm X}T^7 + h^{\phi}_{\rm X}T^{-9} \qquad (2.1) $$

where $H^{\rm SER}_{\rm X}$ is the molar enthalpy of element X at 298.15 K and 10^5 Pa in its standard element reference (SER) state, *i.e.*, α-Am (dhcp) for Am and α-Pu (monoclinic) for Pu, and T is the absolute temperature.

In the present study these Gibbs energy functions are taken from the Scientific Group Thermodata Europe (SGTE) compiled by Dinsdale [26,27]. In the case of pure Pu, the six transitions, α-Pu (monoclinic) $\rightarrow$ β-Pu (body-centered monoclinic) $\rightarrow$ γ-Pu (face-centered orthorhombic) $\rightarrow$ δ-Pu (fcc) $\rightarrow$ δ'-Pu (body-centered tetragonal) $\rightarrow$ ϵ-Pu (bcc) $\rightarrow$ Liquid, are well described energetically with transition temperatures of 124, 215, 320, 463, 483, and 640 ^{o}C, respectively.

For a binary solution phase based on the structure ϕ a simple sublattice model $(\rm Am,Pu)_1$ is considered, and the Gibbs energy is given by

$$ G^{\phi}_{\rm Am,Pu}(c,T) - (1-c)H^{\rm SER}_{\rm Am} - cH^{\rm SER}_{\rm Pu} = (1-c)\ {}^0G^{\phi}_{\rm Am}(T) - c\ {}^0G^{\phi}_{\rm Pu}(T) + RT[(1-c)ln(1-c) + cln(c)] + {}^{\rm xs}G^{\phi}_{\rm Am,Pu}(c,T) \qquad (2.2) $$

where the excess Gibbs energy is given by a Redlich-Kister (RK) polynomial expansion [28] according to

$$ {}^{\rm xs}G^{\phi}_{\rm Am,Pu}(c,T) = c(1-c)L^{\phi}_{\rm Am,Pu}(c,T) \qquad (2.3) $$

where c represents the mole fraction of Pu in the alloy, and $L^{\phi}_{\rm Am,Pu}(c,T)$ is a polynomial function of temperature and composition given by

$$ L^{\phi}_{\rm Am,Pu}(c,T) = \sum_{k=0}^{p} {}^kL^{\phi}_{\rm Am,Pu}(T)(1-2c)^k \qquad (2.4) $$

with $k \leq 1$ in the following assessments.

Besides assessed values for the Gibbs energies of the pure species in their various allotropic forms no experimental information is available for the heats of formation or other thermodynamic data of the Am-Pu alloy system as functions of composition and temperature. Because of this lack of experimental data, the CALPHAD optimization process can only rely on the phase diagram information (mostly from Ref. [6]), unless *ab initio* input from DFT calculations on energetics is considered. Although the DFT results are obtained at 0 K, the number of unknowns is only limited to the temperature-dependent terms that enter the description of the excess Gibbs energies, see Eq. (2.3), and therefore make the assessment possibly more trustworthy.

It is worth noting that since the two species differ by only one valence electron, one should expect weak alloying effects unless localization has a tendency to enhance or cancel out the ordering (or clustering) tendencies. With this in mind, for the fcc solid solution of Am-Pu, the measured lattice constant positively deviates (although weakly) from Vegard's law [5,19], and this fact is usually accompanied by a tendency toward phase separation. In support of this conclusion, and as mentioned in Ref. [25], recent measurements of Am vapor pressure in the Am-Pu binary system points to a slightly positive departure from Raoult's law. Hence, one would expect that a miscibility gap is located at relatively low temperatures in the fcc domain of stability, although experimentally it may be challenging to identify it for two main reasons. First, phase separation is usually a slow kinetics process, especially in the present case since it is expected to take place at low temperatures. And second, the scattering factors of the Pu and Am atoms are almost equals, making the detection of phase separation (or ordering for that matter) very difficult.

Despite the experimental difficulties that are expected for this system, a first tentative phase diagram has been proposed by Ogawa in the early 90's [24] that we are briefly discussing now. Basically, Ogawa applies a regular solution model with interaction parameters derived from the Brewer valence band model [29] that provides a relation between these parameters and the "internal pressures" of the elements. In this assessment, the only phases

that are considered are liquid, bcc, and fcc. The RK parameters introduced in Eq. (2.3) are given in Table I. Note that for the two unaries, Am and Pu, the Gibbs energy functions were taken from Ref. [26] for their observed allotropes and the liquid state, instead of using the free energies of transformation reported in Table 3 of Ogawa's paper. Figure 2 shows the calculated phase diagram with the Thermo-Calc software [30] that indicates complete solid solubility between fcc-Am and fcc-Pu, and also bcc-Am and bcc-Pu at elevated temperatures. Since the RK interactions parameters (which are temperature independent in this model) for each of the three phases are of the order of 1 kJ/mole, it does not come as a surprise that the calculated miscibility gaps obtained by "suspending" all other phases except bcc or fcc, and shown in Fig. 2 are located at very low temperatures, and that the heats of mixing (that also represent the excess Gibbs energies in the present case) for both bcc and fcc phases are extremely small, not exceeding 200-300 J/mole as shown in Fig. 3. Note that the fcc miscibility gap is the only one that is stable when all three phases are considered.

More recently, Kurata [25] published a complete version of the Am-Pu phase diagram. In this study the assessment solely relies on the sparse experimental information on phase diagram discussed in the introduction, and in particular on the finding of a peritectic reaction between the liquid and the bcc and fcc phases in the Pu-rich region of the phase diagram at high temperatures, see Fig. 1a, as reported by Ellinger *et al.* [5]. For the phase diagram assessment, the SGTE data are considered for the pure elements, Am and Pu, and additional guessed data are proposed for the lattice stability values that are needed, *i.e.*, the Gibbs energy of pure Am associated with the various allotropes of Pu (excluding fcc and bcc), and of pure Pu associated with the dhcp phase of Am. The assessed RK interaction parameters and the Gibbs energies associated with the pure elements for all the phases are recalled in Tables I and II, respectively. The resulting Am-Pu phase diagram is shown in Fig. 4. Note that the existence of the peritectic reaction in the Pu-rich region of the phase diagram implies a similar reaction in the Am-rich region. Also, based on this assessment, although a phase separation tendency exists for the bcc phase of Am-Pu with

a maximum temperature of about 180 °C for the metastable symmetric miscibility gap (see dashed line in Fig. 4), a tendency toward order is predicted for the fcc phase of Am-Pu, with a rather high and negative heat of mixing around equi-atomic composition, see Fig. 3. This structure-dependent trend is rather unusual, and hence questions the legitimacy of the assessment.

III. COMPUTATIONAL DETAILS OF *AB INITIO* MODELING AND RESULTS

Since relativistic effects cannot be ignored, the exact muffin-tin orbital (EMTO) electronic-structure method that has been selected makes use of both scalar-relativistic (SR) and fully relativistic (FR) Green's function techniques based on the improved screened Korringa-Kohn-Rostoker (KKR). Spin-orbit interaction, when included, is obtained by solving the four-component Dirac equation [31]. In the EMTO method, the one-electron potential is represented by optimized overlapping muffin-tin (OOMT) potential spheres [32,33], where inside the potential spheres the potential is spherically symmetric, whereas it is constant between the spheres. The radii of the potential spheres, the spherical potentials inside the spheres, and the constant value in the interstitial region are determined by minimizing (i) the deviation between the exact and overlapping potentials, and (ii) the errors caused by the overlap between the spheres. Within the EMTO formalism, the one-electron states are calculated exactly for the OOMT potentials. As an output of the EMTO calculations, one can determine the self-consistent Green's function of the system and the complete non-spherically symmetric charge density. Finally, the total energy is calculated using the full charge-density technique [34]. EMTO is combined with the coherent potential approximation (CPA) for the calculation of the total energy of chemically random alloys [35].

The calculations are performed for a basis set including valence *spdf* orbitals. For the electron exchange and correlation energy functional, the generalized gradient approximation (GGA) is considered [36]. Integration over the Brillouin zone is performed using the special k-point technique [37]. The screening constants that are required to describe the Coulomb

screening potential and the energy [38–40], are determined from super-cell calculations using the locally self-consistent Green function (LSGF) method [41]. The α and β screening constants, see Refs. [38,39] for details, are found to be 1.14 and 1.00, and 1.07 and 1.00, for bcc and fcc Am-Pu, respectively. The Am-Pu alloys have been modeled within the disordered local moment approximation that leads to a paramagnetic solution, see Refs. [10,13] for details. The moments of the density of states (DOS), needed for the kinetic energy and the valence charge density, are calculated by integrating the Green function over a complex circular energy contour (with a 2.5 Ry diameter) using a Gaussian integration technique with 30 points on a semi-circle enclosing the occupied states. The equilibrium atomic density is obtained from a Murnaghan [42] fit to the total energy versus lattice constant curve.

For the elemental metals, the most accurate and fully relativistic calculations are performed using an all-electron approach where the relativistic effects, including spin-orbit coupling, are accounted for. Although unable to model disorder in the CPA sense it provides important information for the metals, and also serves to confirm the CPA calculations mentioned above. For this purpose we use a version of the FPLMTO presented in Ref. [43], and the "full potential" in FPLMTO refers to the use of non-spherical contributions to the electron charge density and potential. This is accomplished by expanding the charge density and the potential in cubic harmonics inside non-overlapping muffin-tin spheres and in a Fourier series in the interstitial region. We use two energy tails associated with each basis orbital, and for U's semi-core $6s$ and $6p$ states and valence states ($7s$, $7p$, and $5f$) these pairs are different. With this "double basis" approach we use a total of six energy tail parameters and a total of 12 basis functions per atom. Spherical harmonic expansions are carried out up to $l_{max} = 6$ for the basis, potential, and charge density. As in the case of the EMTO method, GGA is used for the electron exchange-correlation approximation. Finally, a special quasi-random structure (SQS) method, utilizing a 16-atom super-cell, was used to treat compositional disorder [44], so the results could be compared with those obtained with EMTO-CPA.

These methodologies have been successfully applied to the two elements, Am [18,16] and

Pu [9–12], and also to fcc-based Am-Pu alloys from pure Pu to equi-atomic composition [19]. More recently a study of the trend in phase formation for bcc-based Pu-X (X=U,Np,Am,Cm) has shown that except for Pu-U, that displays a tendency towards bcc phase formation (*i.e.*, a negative heat of formation), all the other systems exhibit a tendency towards phase separation (*i.e.*, a positive heat of formation) [45].

To confirm the proximity of Pu and Am in the periodic table, we show in Fig. 5 typical densities of states (DOS) for a chemically random fcc-based Am-Pu alloy at equi-atomic composition, and at the theoretical equilibrium atomic volume of 0.027314 nm^3. Despite the fact that the $6s$ and $6p$ partial DOS are fairly localized far below the Fermi energy (around -2.0 and -1.2 Ry respectively), their contribution to the calculated total energy cannot be ignored by treating them as core states. The hybrid states centered around the Fermi energy are mostly made of $5f$ (dominating) and $6d$ states, and the contribution of Am and Pu to the total DOS are rather similar, with a slightly higher DOS associated with Pu at the Fermi energy. The main effect of adding Am to Pu is to move the Fermi energy at higher energy (to the right), and therefore to change rather substantially the electronic DOS at the Fermi energy since this occurs in a region where a pseudo-gap exists. Experimentally the electronic spectra of ground-state Am metal shows a wider pseudo-gap with a peak structure about 0.25 Ry below the Fermi level [46] but for the alloy system it may be substantially different. Our result could be verified by carrying out specific heat measurements as functions of alloy composition, tracking the electronic γ contribution to heat capacity, or by direct X-ray spectroscopy.

Fig. 6 displays the results from FR-EMTO-CPA calculations for the equilibrium atomic volume and bulk modulus in the entire range of alloy composition for the chemically random fcc phase of Am-Pu. Our results confirm the positive departure of the atomic volume from Zen's law observed experimentally [5], and therefore the possible existence of a miscibility gap in the solid fcc phase at rather low temperatures (since the departure from linearity is small). At the same time, the addition of Am to a Pu matrix tends to decrease cohesion as indicated by the negative departure from linearity for the bulk modulus. In Fig. 7, the

heat of mixing (or excess Gibbs free energy at 0 K) is shown versus alloy composition for both the fcc and bcc phases of the random solid solutions of Am-Pu. For both phases, the positive heats of mixing, not exceeding 7 kJ/mole suggest a (rather small) tendency towards phase separation. However, when compared to Fig. 3, the difference between the phenomenologically assessed data and our first-principles derived results is quite significant not only quantitatively but also qualitatively when compared with the results of Kurata [25], since in the latter case the heats of mixing associated with the bcc and fcc phases have opposite signs. Hence in the following section we will make use of these heats of mixing evaluated at 0 K to initiate the CALPHAD assessment of the Am-Pu phase diagram. The RK description of these *ab initio* predicted excess Gibbs energies at 0 K (in J/mole) is given by

$$\begin{aligned} L^{\rm fcc}_{\rm Am,Pu}(c,0K) &= 25855.4 - 4906.3\ (1-2c) \\ L^{\rm bcc}_{\rm Am,Pu}(c,0K) &= 21157.8 - 1518.3\ (1-2c) \end{aligned} \tag{3.1}$$

Before closing this section, let us present the results of FR-EMTO calculations that have been performed to evaluate the structural energy differences for the pure elements Am and Pu at equilibrium. Note that in the case of Am, the anti-ferromagnetic (AF) structure is the ground state as compared to the paramagnetic state (treated within the disordered local moment (DLM) approximation), and also to other structures such as dhcp and hcp with ABACABAC and ABAB stacking sequence along the (0001) direction (although for these two cases, optimization was not carried out to minimize the energy with respect to the c/a axial ratio). The results (in J/mole) for Am are:

$$\begin{aligned} \Delta E^{\rm fcc(DLM)-fcc(AF)}_{\rm Am} &= +1,683.0 \\ \Delta E^{\rm dhcp(DLM)-fcc(AF)}_{\rm Am} &= +1,503.1 \\ \Delta E^{\rm hcp(DLM)-fcc(AF)}_{\rm Am} &= +1,6711.4 \\ \Delta E^{\rm bcc(DLM)-fcc(AF)}_{\rm Am} &= +1,605.5 \end{aligned} \tag{3.2}$$

and for Pu

$$\Delta E_{\rm Pu}^{\rm hcp-fcc} = +2,944.5$$
$$\Delta E_{\rm Pu}^{\rm dhcp-fcc} = +1,680.3$$
$$\Delta E_{\rm Pu}^{\rm fcc-bcc} = -3,516.9 \qquad (3.3)$$

In the case of Am, the structural energy differences are quite small (of the order of 1 kJ/mole) and for Pu, dhcp is more stable than hcp, and fcc is the most stable among the three considered stacking sequences. It is interesting to compare these *ab initio* results to those proposed by SGTE [26]. In the latter case, to obtain the data extrapolated at 0 K, it was assumed that the Gibbs energy G of a phase is given in a polynomial form that satisfies the version of the third law of thermodynamics according to which the entropy is equal to 0 at 0 K (the so-called Planck's version of the third law [47]), hence $G = a + bT^2 + cT^3$. Based on this extrapolating scheme with Gibbs energies calculated according to their definition in Ref. [26] in the {200,400} K temperature range, the SGTE energy differences (in J/mole) are for Am:

$$\Delta E_{\rm Am}^{\rm dhcp-fcc} = -1,713.4$$
$$\Delta E_{\rm Am}^{\rm fcc-bcc} = -4,024.1 \qquad (3.4)$$

and for Pu

$$\Delta E_{\rm Pu}^{\rm fcc-bcc} = -2,451.6 \qquad (3.5)$$

These results compare favorably with the *ab initio* predictions, except perhaps for the structural energy difference between fcc and bcc in the case of Am. In the next section, the *ab initio* result for dhcp-Pu will be used for the CALPHAD assessment of the Am-Pu phase diagram. In passing, it is worth pointing out an abnormality in the SGTE data (despite the fact that usually they are considered valid only above room temperature) for pure Pu that describes the Gibbs energy difference between the bcc (or ϵ) phase and the liquid as illustrated in Fig. 8. This difference points out a liquid phase that is more stable than bcc at low temperatures (below about 320 K). This "reentrant" liquid has no physical meaning,

and thus question is raised about the validity of the proposed SGTE Gibbs energies for the bcc and liquid phases.

IV. ASSESSMENT AND RESULTS

The phase diagram assessment will proceed in two steps as follows. First, only the liquid, bcc, and fcc phases will be considered and the energetic data cast in a RK format for the heats of mixing at 0 K deduced from the results displayed in Fig. 7 will be used, see Eqs. 3.1, to assess the high-temperature portion of the Am-Pu phase diagram with experimental information displayed in Fig. 1b. Second, the assessed data for the fcc solid solution will be used with the experimental information on the low-temperature phases. However, since this information may not reflect equilibrium data, especially on the Pu-rich side of the phase diagram (below 320 °C) because of sluggish kinetics, not a high level of certainty will apply to this part of the assessment. For the second part, the heats of formation of Am in the α, β, γ, and δ' structures of Pu, and of Pu in the α-Am (dhcp) structure have to be estimated since they are not given in the SGTE database [26,27]: the results are shown in Table II. For the liquid, bcc, fcc, and dhcp (or α-Am) phases the excess Gibbs energies given by Eqs. 2.3 and 2.4 are expressed by a first-order RK polynomial ($k \leq 1$), whereas for all other phases (α-Pu, β-Pu, γ-Pu, and δ'-Pu) they are simply described by a zero-th order RK polynomial ($k = 0$). As illustrated in Pelton's work [48], since the solidus-liquidus lines (bcc-liquid two-phase region) exhibit a negative curvature, one would expect the first parameter of the RK polynomial expansions for the bcc and liquid phases to satisfy: ${}^0L^{\rm bcc}_{\rm Am,Pu} < {}^0L^{\rm liq}_{\rm Am,Pu}$, a constraint that was accounted for in the optimization procedure.

For the first step where only the three high-temperature phases are considered the results of the optimization obtained with Thermo-Calc and its PARROT module [30] are shown in Fig. 9 together with the experimental data on the fcc-bcc two phase equilibrium and the the solidus-liquidus region suggested by the experimental work of Shushakov *et al.* [6]. It is worth noting that with the present thermodynamics both the fcc and bcc phases display

asymetric miscibility gaps (stable for fcc and unstable for bcc) at low temperatures with maximum temperature of 138.9 and 235.3 °C and associated composition of 72.1 and 75.8 at.% Pu, respectively. With temperature-independent $L_{\mathrm{Am,Pu}}$ as given by Eq. 3.1 straight from the *ab initio* results, these miscibility gaps would be centered around 55.2 and 61.9 at.% Pu with maximum temperatures of 1013.6 and 1392.4 °C for the fcc and bcc phases, respectively. The temperature-dependent contribution to the RK interactions that seems a bit large for both phases may simply reflect their stabilization by entropy effect.

For the second step where all phases are considered, the calculated phase diagram is displayed in Fig. 10, and the details of the thermodynamic assessment are reported in Tables I and II. Although the third law of thermodynamics, especially in its Planck version [47], is more of a postulate, its application precludes the existence of a fcc-based solid solution down to zero temperature. In the present case a low-lying eutectoid decomposition takes place according to the reaction (δ-Pu, β-Am) $\rightarrow$ (α-Pu) + (α-Am) at 104 °C with compositions (in at.% Pu) of 31.1, $\sim$ 100, and 2.2, respectively. It is also worth noting that a small region of fcc miscibility gap, shown in the inset of Fig. 10 and mentioned in the previous paragraph, survives and leads to an eutectoid reaction at 136 °C that involves two fcc phases and β-Pu. The final assessed phase diagram accounts for the existence of a high-temperature bcc solid solution, and a domain of stability of a dhcp (A3')-based solid solution in the Am rich-side of the phase diagram, with a two-phase region (fcc+dhcp) in accordance with the findings of Shushakov *et al.* [6], and as expected from the fundamental laws of thermodynamics.

It is interesting to ask how much it would take to have a peritectoid reaction (ϵ-Pu, γ-Am) $\rightarrow$ (δ-Pu,β-Am) + Liquid, as suggested by Ellinger *et al.* [5], and shown in Fig. 1a. To generate such a feature in the phase diagram requires a positive contribution to the excess Gibbs energy of the bcc phase, so to make it less stable than the liquid phase. By substituting the $L^{\mathrm{bcc}}_{\mathrm{Am,Pu}}$ by $L^{\mathrm{bcc}}_{\mathrm{Am,Pu}} + 3000 + 1000(1-2c)$ to account for the peritectic reaction that exists in the Pu-rich portion of the phase diagram at high temperature, keeping all other assessed data the same, the phase diagram shown in Fig. 11 is obtained.

With these new RK parameters for the bcc solid solution, the peritectoid reaction (δ-Pu) $\rightarrow$ Liquid + (γ-Am) takes place at 670 ^{o}C with compositions (in at.% Pu) of 90.4, 96.0, and 94.7, respectively. It is also important to note that to insure compatibility with the existence of the high-temperature allotrope of Am (γ-Am or bcc), a second peritectoid reaction should take place on the Am-rich side of the phase diagram, namely (δ- Pu)$\rightarrow$Liquid+(γ-Am) at 1126 ^{o}C with compositions (in at.% Pu) of 7.7, 9.2, and 6.8, respectively, as illustrated in Fig. 11. This finding shows that the high-temperature part of the Am-Pu phase diagram is extremely sensitive to the thermodynamic data and hence to the impurity content. It is then fair to say that the two phase diagrams displayed in Figs. 10 and 11 are possible representations of the stability properties of the Am-Pu system, although the most recent one proposed by Shushakov *et al.* [6], because of the more thorough experimental work, may be given more attention. Further improvement to the thermodynamic description of this system will require additional experiments, in particular differential scanning calorimetry (DSC) and differential thermal analysis (DTA) combined with high-temperature X-ray structure analysis. However, this preliminary study provides some initial thermodynamic data for this system that can also be compared with other theoretical modeling.

V. CONCLUSION

A thermodynamic assessment of the Am-Pu phase diagram in the entire range of alloy composition was performed. Consistent finding between the "Russian" most updated results [6] and modeling was achieved for the upper part of the phase diagram, with additional features such as the two-phase region between fcc and dhcp-based solid solution in the Am-rich part of the phase diagram, and a low-lying eutectoid phase decomposition δ-solid solution $\rightarrow$ α-Pu + α-Am solid solution. The experimental evidence of a positive departure from Vegard's law together with the zero-temperature energetics predicted from *ab initio* calculations, seem to clearly suggests a phase separating tendency for the fcc phase, and consequently also for the bcc phase. To find an agreement with the early results of Ellinger

et al. [5], it was shown that a slight destabilization of the bcc solid solution was required, thus generating a peritectoid reaction on the Pu side of the phase diagram, and to make both the Pu-rich and Am-rich sides of the phase diagram compatible, a second peritectoid reaction was expected on the Am-rich side as well. A more detailed assessment of the Am-Pu phase diagram is at present prohibited by the lack of thermodynamic data and accurately determined phase boundaries. These two possible phase diagrams and the minor difference in the thermodynamics that can explain them may point to a high sensitivity to impurity effect. However, since sample preparation is challenging, the present CALPHAD assessment delineates some alloy compositions, namely around 80 and 90 at.% Pu, to further confirm the existence or not of a domain of stability of a bcc solid solution in the entire range of alloy composition or a peritectoid reaction, respectively. In Fig. 12 the molar enthalpy and its derivative with respect to temperature associated with each phase (fcc, bcc, and liquid) is shown as a function of temperature for the two proposed phase diagrams at 80 and 90 at.% Pu. Differential thermal analysis should be able to qualitatively distinguish between the two cases whereas differential scanning calorimetry should provide a quantitative determination of the heats of transformation. Nevertheless, initial thermo-chemical results derived from the optimization process are now available to design critical experiments, and obtain a more accurate representation of the thermostatics of the Am-Pu system. Finally, on a more technical side, this study has shown that the appropriate tools are in place, and if new qualified experimental results are made available, the optimization procedure could be used quite easily to fine-tune the present results.

Acknowledgments

This work was performed under the auspices of the U.S. Department of Energy by Lawrence Livermore National Laboratory under Contract DE-AC52-07NA27344.

*Corresponding author. Tel.: +1 925 422 9925; fax: +1 925 423 7496 E-mail address: turchi1@llnl.gov (P.E.A. Turchi).

REFERENCES

[1] US DOE Nuclear Energy Research Advisory Committee and the Generation IV International Forum, *A Technology Roadmap for Generation IV Nuclear Energy Systems*, US Department of Energy Report, December 2002.

[2] *Phase Diagram of Binary Actinide Alloys*, Monograph Series on Alloy Phase Diagrams, vol. **11**, M.E. Kassner and D.E. Peterson eds. (ASM International, Materials Park, OH, 1995).

[3] T.B. Massalski, ed., *Handbook of Alloy Phase Diagrams*, (ASM International, Materials Park, OH, 1990), 3 volumes.

[4] H. Okamoto, J. of Phase Equilibria **20**, 451 (1999); and *A-B-C Phase Diagram*, ASM Alloy Phase Diagrams Center, P. Villars, editor-in-chief; H. Okamoto and K. Cenzual, section editors; http://www1.asminternational.org/AsmEnterprise/APD, ASM International, Materials Park, OH, 2006.

[5] F.H. Ellinger, K.A. Johnson, and V.O. Struebing, J. of Nucl. Mater. **20**, 83 (1966).

[6] V.D. Shushakov, N.S. Kosulin, and N.T. Chebotarev, Problems of Nuclear Science and Engineering, Series Materials Science and New Materials (3) (1990) 14.

[7] A.G. Seleznev, N.S. Kosulin, and V.D. Shushakov, Phys. Met. Metall. **44**, (3) 180 (1978).

[8] A.G. Seleznev, V.D. Shushakov, and N.S. Kosulin, Phys. Met. Metall. **46**, (5) 193 (1979).

[9] P. Söderlind, Europhys. Lett. **55**, 525 (2001).

[10] P. Söderlind, A. Landa, and B. Sadigh, Phys. Rev. B **66**, 205109 (2002).

[11] P. Söderlind and B. Sadigh, Phys. Rev. Lett. **92**, 185702 (2004).

[12] P. Söderlind, Phys. Rev. B **77**, 085101 (2008).

[13] A. Landa and P. Söderlind, J. Alloys Compd. **354**, 99 (2003).

[14] S.Y. Savrasov, G. Kotliar, and E. Abrahams, Nature **410**, 793 (2001).

[15] X. Dai, S.Y. Savrasov, G. Kotliar, A. Migliori, H. Ledbetter, and E. Abrahams, Science **300**, 953 (2003).

[16] P. Söderlind, K.T. Moore, A. Landa, and J.A. Bradley, Phys. Rev. B in press (2011).

[17] J.C. Lashley, *et al.*, Phys. Rev. B **72**, 054416 (2005).

[18] P. Söderlind and A. Landa, Phys. Rev. B **72**, 024109 (2005).

[19] A. Landa and P. Söderlind, J. Alloys Compd. **376**, 62 (2004).

[20] A. Landa, P. Söderlind, and L. Vitos, J. Alloys Compd. **444-445**, 296 (2007); P. Söderlind, A. Landa, and W.G. Wolfer, J. Comput. Aided Mater Des. **14**, 349 (2007).

[21] L. Kaufman and H. Bernstein, *Computer Calculation of Phase Diagrams with Special Reference to Refractory Metals* (Academic Press, New York, 1970).

[22] N. Saunders and A.P. Miodownik, *CALPHAD, Calculation of Phase Diagrams: A Comprehensive Guide*, Pergamon Materials Series, vol. **1**, ed. by R.W. Cahn (Pergamon Press, Oxford, 1998).

[23] *CALPHAD and Alloy Thermodynamics*, ed. by P.E.A. Turchi, A. Gonis, and R.D. Shull (TMS Publication, Warrendale, PA, 2002); and references therein.

[24] T. Ogawa, J. of Alloys and Comp. **194**, 1 (1993).

[25] M. Kurata, Mat. Sci. Eng. IOP Conference Series **9**, 012023 (2010).

[26] A. Dinsdale, CALPHAD **15**, 317 (1991).

[27] I. Ansara and B. Sundman, *The Scientific Group Thermodata Europe*, P.S. Glaeser ed., Computer Handling and Dissemination of Data (Elsevier Science Pub. Co., Amsterdam, 1987).

[28] O. Redlich and A. Kister, Ind. Eng. Chem. **40**, 345 (1948).

[29] L. Brewer and R.H. Lamoreaux, At. Energy Rev., Spec. Issue No7, 11-194 (1980).

[30] The Thermo-Calc application software is a product of Thermo-Calc AB; B. Sundman, B. Jansson, and J.-O. Andersson, CALPHAD **9** (4), 153 (1985); cf. also http://www.thermocalc.se.

[31] L.V. Pourovskii, A.V. Ruban, L. Vitos, H. Ebert, B. Johnasson, and I.A. Abrikosov, Phys. Rev. B **71** 094415 (2005).

[32] L. Vitos, Phys. Rev B **64**, 014107 (2001).

[33] L. Vitos, *Computational Quantum Mechanics for Materials Engineers: The EMTO Method and Application* (Springer, London, 2007).

[34] J. Kollár, L. Vitos, and H.L. Skriver, in: H. Dreyssé (Ed.), *Electronic Structure and Physical Properties of Solids: The Uses of the LMTO Method*, Lecture Notes in Physics (Springer, Berlin, 2000), pp. 85-113.

[35] L. Vitos, I.A. Abrikosov, and B. Johansson, Phys. Rev. Lett. **87**, 156401 (2001).

[36] J.P. Perdew, K. Burke, and M. Ernzerhof, Phys. Rev. Lett. **77**, 3865 (1996).

[37] D.J. Chadi and M.L. Cohen, Phys. Rev. B **8**, 5747 (1973); S. Froyen, Phys. Rev B **39**, 3168 (1989).

[38] A.V. Ruban and H.L. Skriver, Phys. Rev. B **66**, 024201 (2002).

[39] A.V. Ruban, S.I. Simak, P.A. Korzhavyi, and H.L. Skriver, Phys. Rev. B **66**, 024202 (2002).

[40] A.V. Ruban, S.I. Simak, S. Shallcross, and H.L. Skriver, Phys. Rev. B **67**, 214302 (2003).

[41] I.A. Abrikosov, S.I. Simak, B. Johansson, A.V. Ruban, and H.L. Skriver, Phys. Rev. B **56**, 9319 (1997).

[42] F.D. Murnaghan, Proc. Natl. Acad. Sci. U.S.A. **30**, 244 (1944).

[43] J.M. Wills, O. Eriksson, M. Alouani, and D.L. Price, in: H. Dreyssé (Ed.), *Electronic Structure and Physical Properties of Solids: The Uses of the LMTO Method*, Lecture Notes in Physics (Springer, Berlin, 2000), pp.148-167.

[44] A. Zunger, S.H. Wei, L.G. Ferreira, and J.E. Bernard, Phys. Rev. Lett. **65**, 353 (1990).

[45] A. Landa, P. Söderlind, P.E.A. Turchi, L. Vitos, O.E. Peil, and A.V. Ruban, J. of Nucl. Mater. **408**, 61 (2011).

[46] T. Gouder, P.M. Oppeneer, F. Huber, F. Wastin, and J. Rebizant, Phys. Rev. B **72**, 115122 (2005).

[47] M. Planck, *Treatise on Thermodynamics*, (Dover Publications, Inc. New York, 1945).

[48] A.D. Pelton, in *Physical Metallurgy*, 3rd edition, ed. by R. W. Cahn and P. Haasen (Elsevier Science, Amsterdam, 1983), p. 328.

TABLES

TABLE I. Assessed Redlich-Kister (RK) interaction parameters for Am-Pu (in J/mole, and with temperature T in Kelvin). For some phases the excess Gibbs energy is expressed by more than one RK parameter. For the present work, we only report the results for the final assessment with all phases considered.

Phase	Ogawa [24]	Kurata [25]	Present Work
liquid	+1177	+5495.9-1.7762T	+39560.1-55.856T
	-141.5		+3281.4-4.4924T
bcc	+1026	+7528.57	+25855.4-44.631T
	-127.1	+2.7353	-4906.3-0.975T
fcc	+1280	-22630+26.36T	+21157.8-40.723T
	-127.1	-6091	-1518.3-3.885T
		+0.13367	
α-Am	N/A	+5000	+13362.0-22.212T
		+6981.4-3.298T	
α-Pu	N/A	+5000	+31573.2-39.159T
β-Pu	N/A	+5000	+20502.3-11.335T
γ-Pu	N/A	+5000	+36659.7-43.919T
δ'-Pu	N/A	+5000	+37000-44T

TABLE II. Gibbs energies of the pure elements (in J/mole).

Phase	Kurata [25]	Present Work
$G_{\mathrm{Am}}^{\beta\text{-Pu}}$	$+5000+G_{\mathrm{Am}}^{\alpha\text{-Am}}$	$+5000+G_{\mathrm{Am}}^{\alpha\text{-Am}}$
$G_{\mathrm{Am}}^{\gamma\text{-Pu}}$	$+5000+G_{\mathrm{Am}}^{\alpha\text{-Am}}$	$+5000+G_{\mathrm{Am}}^{\alpha\text{-Am}}$
$G_{\mathrm{Am}}^{\delta'\text{-Pu}}$	$+5000+G_{\mathrm{Am}}^{\alpha\text{-Am}}$	$+5000+G_{\mathrm{Am}}^{\alpha\text{-Am}}$
$G_{\mathrm{Pu}}^{\alpha\text{-Am}}$	$+5000+G_{\mathrm{Pu}}^{\delta\text{-Pu}}$	$+1680+G_{\mathrm{Pu}}^{\delta\text{-Pu}}$

FIGURES

FIG. 1. "American" (a) from Refs. [2–5], and "Russian" (c), redrawn from Ref. [6], versions of the Am-Pu phase diagram. In the bottom phase diagram the empty, half-full, and full circles refer to single phase, two-phase region, and results from differential thermal analysis, respectively.

FIG. 2. (Color online) Ogawa's assessment of the Am-Pu phase diagram according to the Brewer model, from Ref. [24]. Only the liquid, bcc, and fcc phases are considered.

FIG. 3. (Color online) Heats of mixing (in J/mole) of fcc (empty circle) and bcc (full circle)-based Am-Pu alloys versus composition according to (solid lines) Ogawa's Brewer-based assessment [24] and (dashed lines) Kurata's CALPHAD assessment [25] of the Am-Pu phase.

FIG. 4. (Color online) CALPHAD assessment of the Am-Pu phase diagram from Kurata's assessment [25]. The metastable bcc miscibility gap is indicated by a dashed line.

FIG. 5. (Color online) Total and partial electronic structure densities of states of fcc-based $Am_{50}Pu_{50}$.

FIG. 6. (Color online) Calculated atomic volume, in nm^3 (a) and bulk modulus in GPa (b) of fcc-based Am-Pu alloys versus composition. In (a) the squares are the experimental data from Ref. [5].

FIG. 7. (Color online) Calculated heats of mixing (in J/mole) of fcc (empty circle) and bcc (full circle)-based Am-Pu alloys versus Pu composition based on the FR-EMTO-CPA method. The squares correspond to the results from the FPLMTO-SQS approach for the bcc phase. The lines are a fit to the data by a Redlich-Kister polynomial of second order.

FIG. 8. (Color online) Calculated Gibbs energy differences between various phases of pure Pu according to the SGTE data [26]. The two arrows indicate that the liquid phase is more stable than bcc below 320 K and above 913 K.

FIG. 9. (Color online) Partial CALPHAD assessment of the Am-Pu phase diagram with input from *ab initio*. Phases other than liquid, bcc, and fcc have not been considered. The red squares (blue circles) are the data describing the solidus- liquidus and fcc-bcc phase equilibria, respectively, collected from the experimental phase diagram given in Fig. 1c.

FIG. 10. (Color online) Final CALPHAD assessment of the Am-Pu phase diagram with input from *ab initio*.

FIG. 11. (Color online) Re-evaluation of the Am-Pu phase diagram by assuming a bcc solid solution even less stable than the liquid at high temperature.

FIG. 12. (Color online) Molar enthalpy H and its derivative dH/dT and versus temperature for Am-Pu alloys with 80 (top) and 90 (bottom) at.% Pu. Part of the figure (in black), referred to 1, is associated with the phase diagram given in Fig. 10 whereas the other part (in red dashed line) is with the one from Fig. 11.

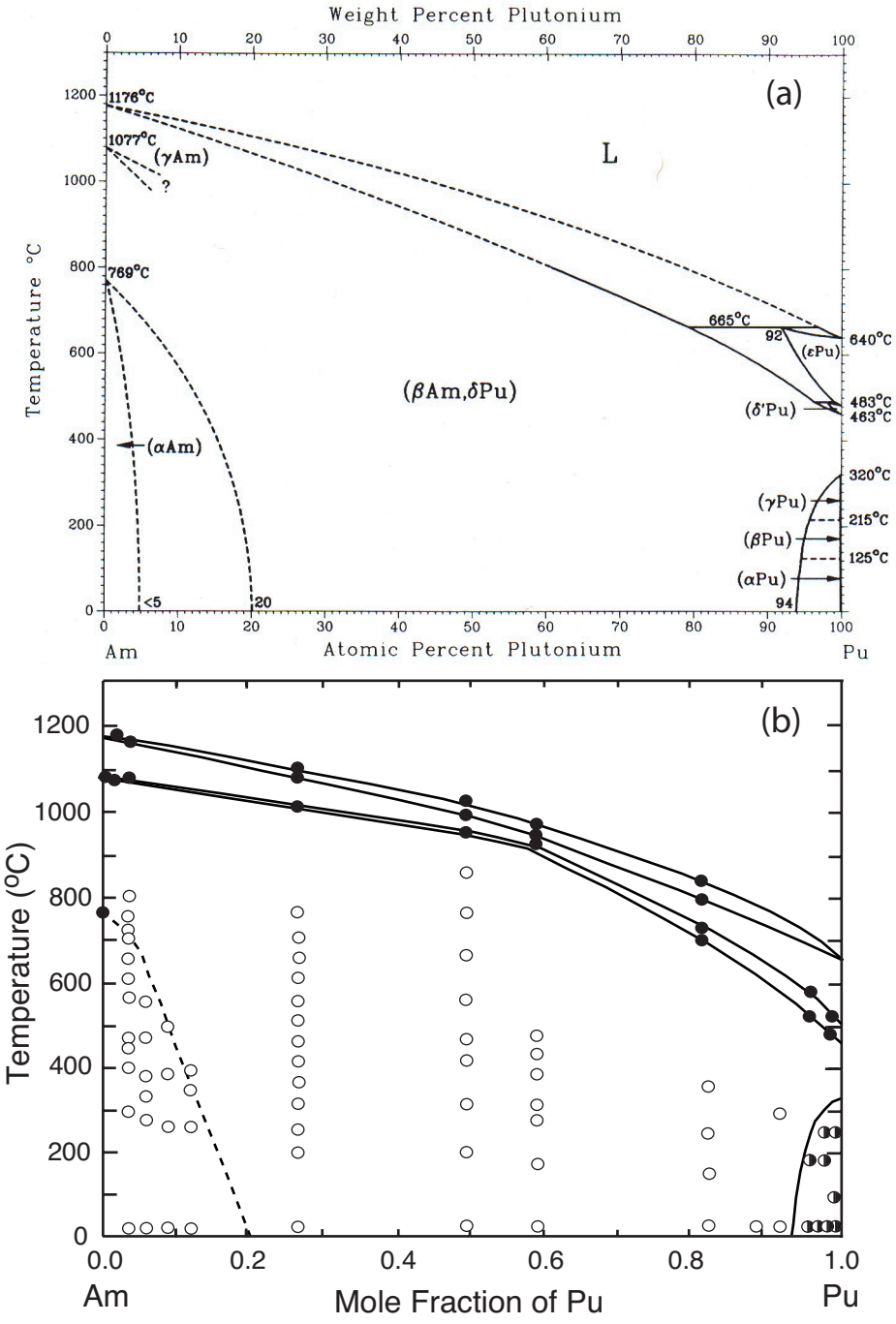

FIG. 1. Turchi *et al.*

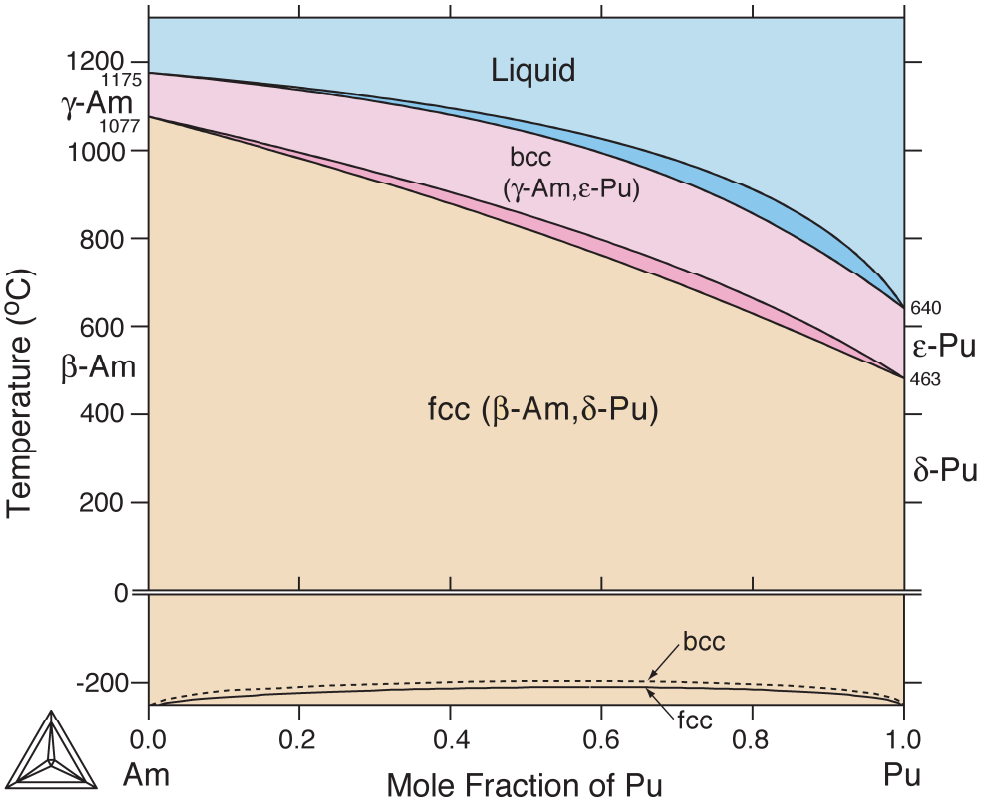

FIG. 2. Turchi *et al.*

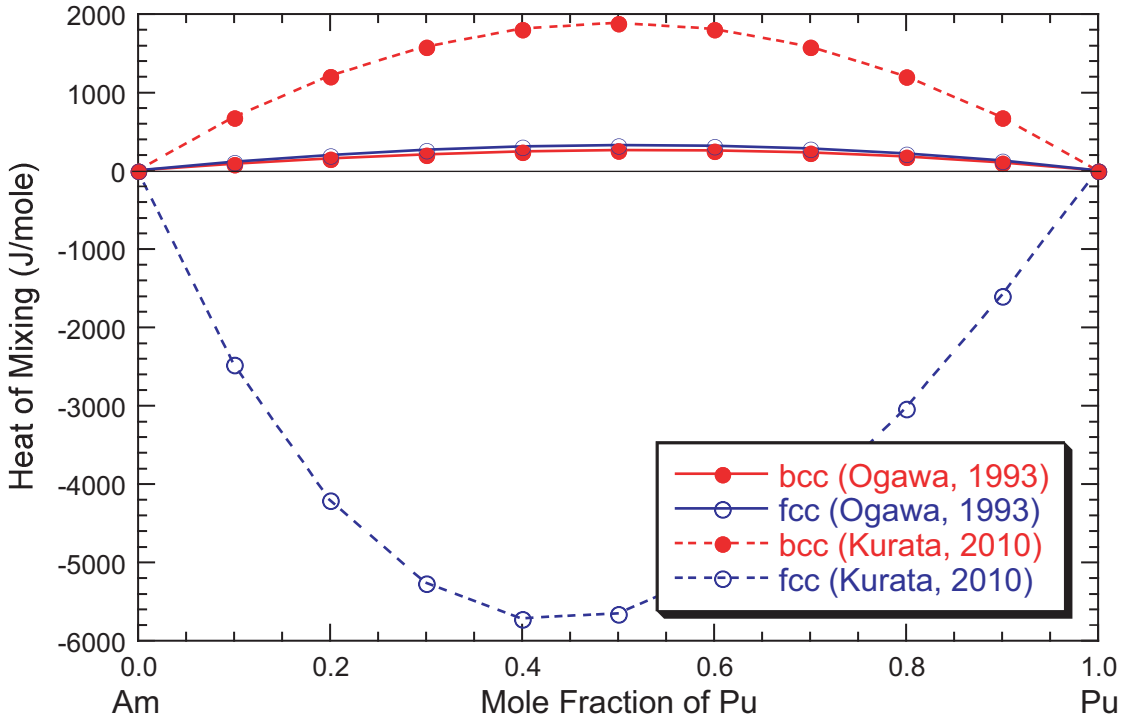

FIG. 3. Turchi *et al.*

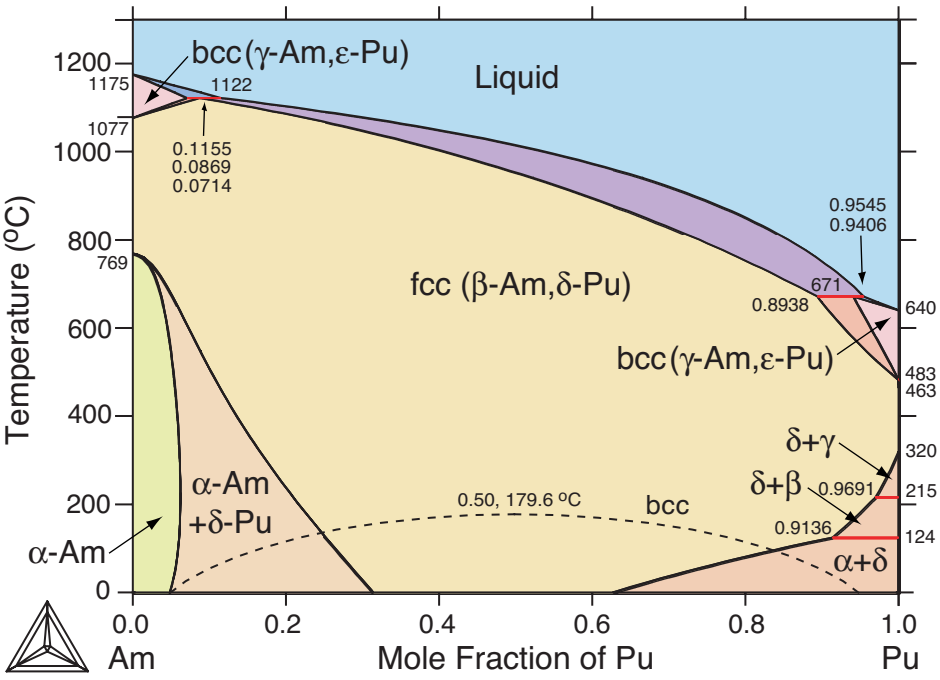

FIG. 4. Turchi *et al.*

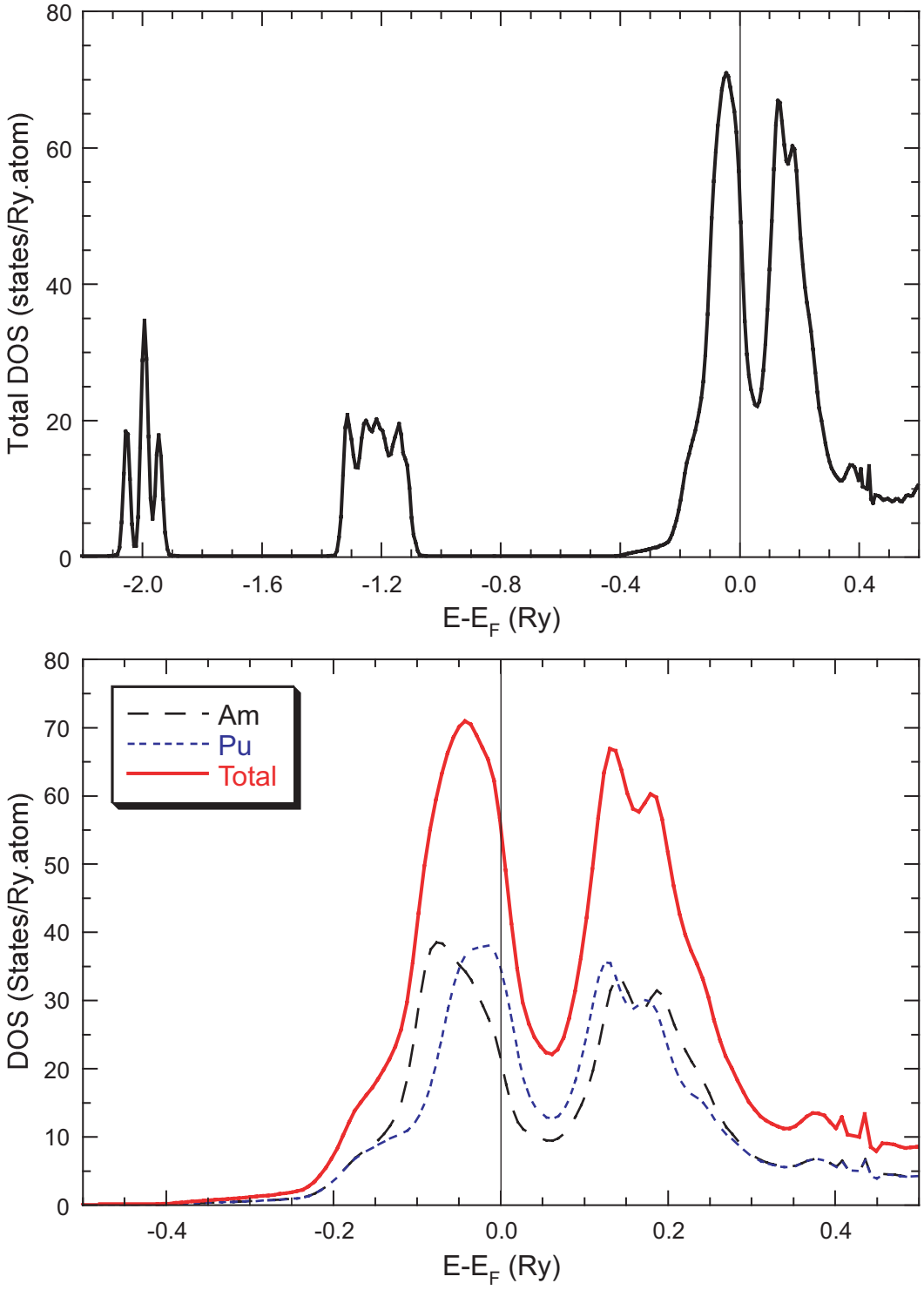

FIG. 5. Turchi *et al.*

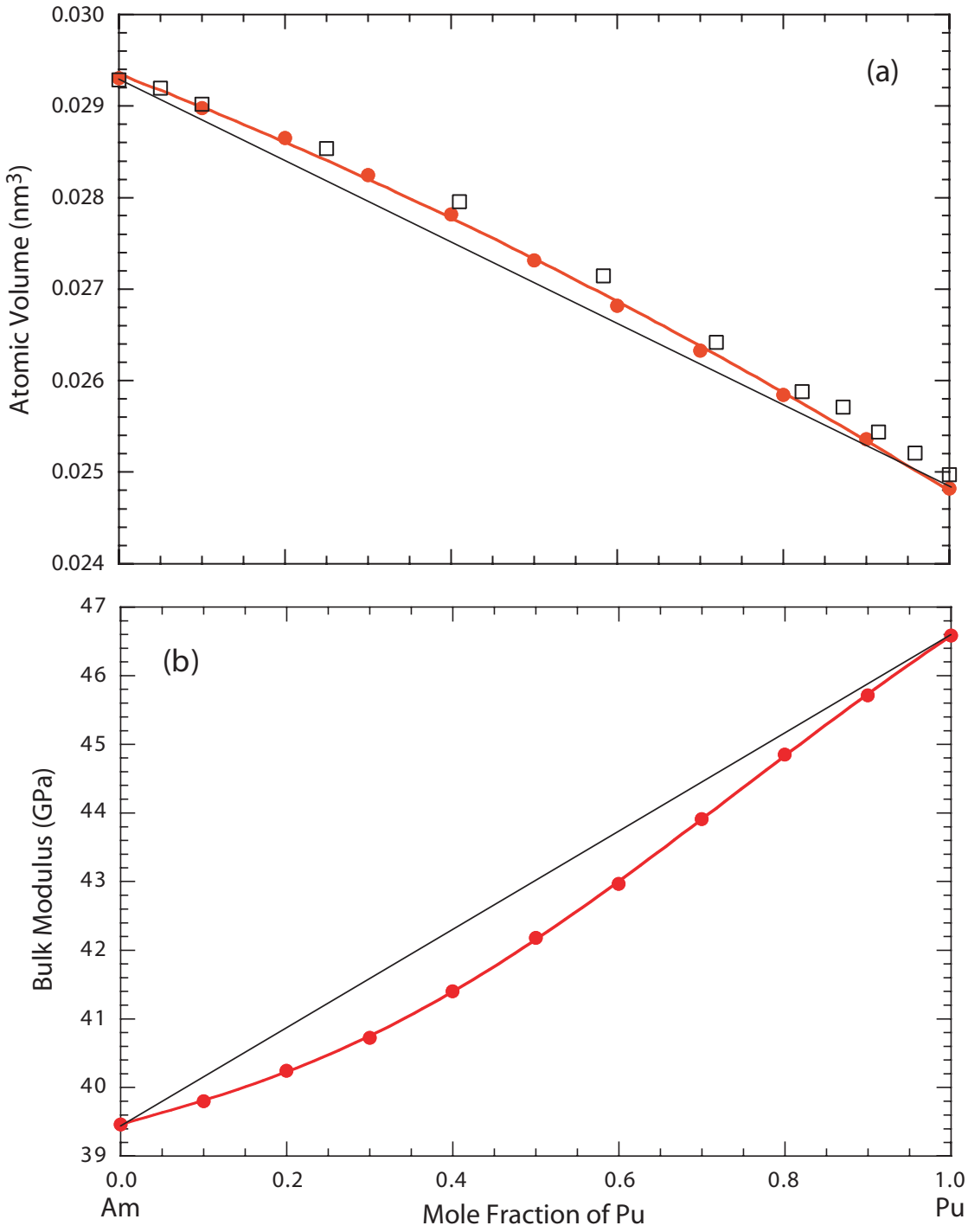

FIG. 6. Turchi *et al.*

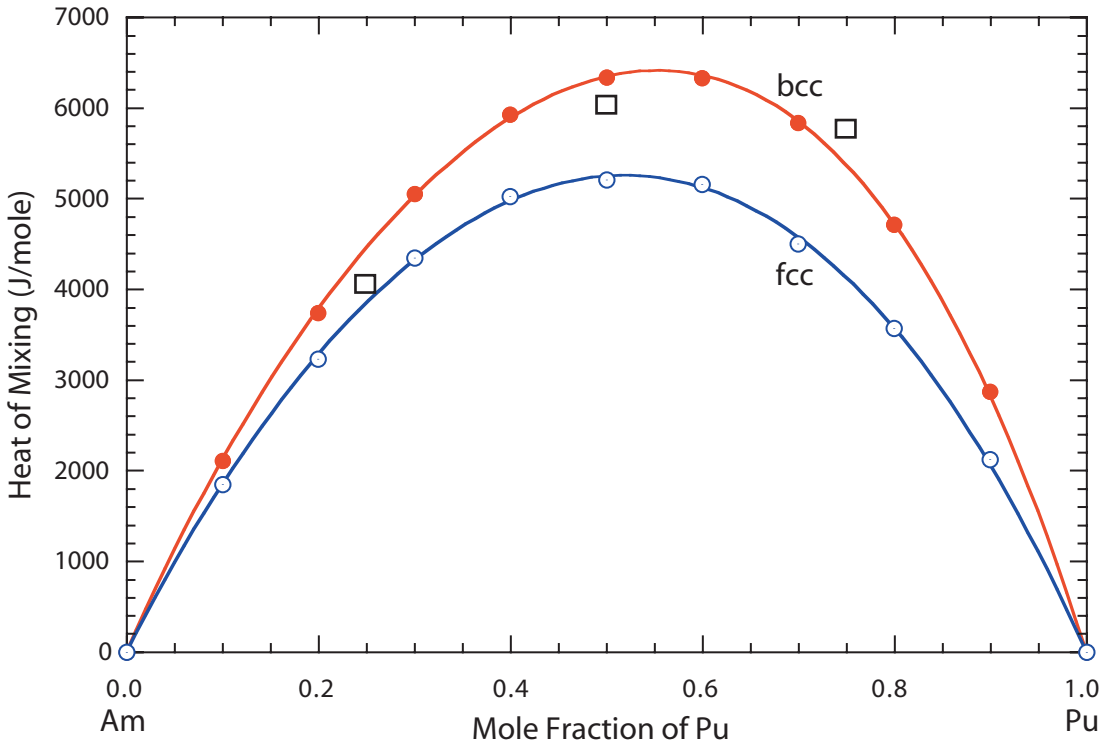

FIG. 7. Turchi *et al.*

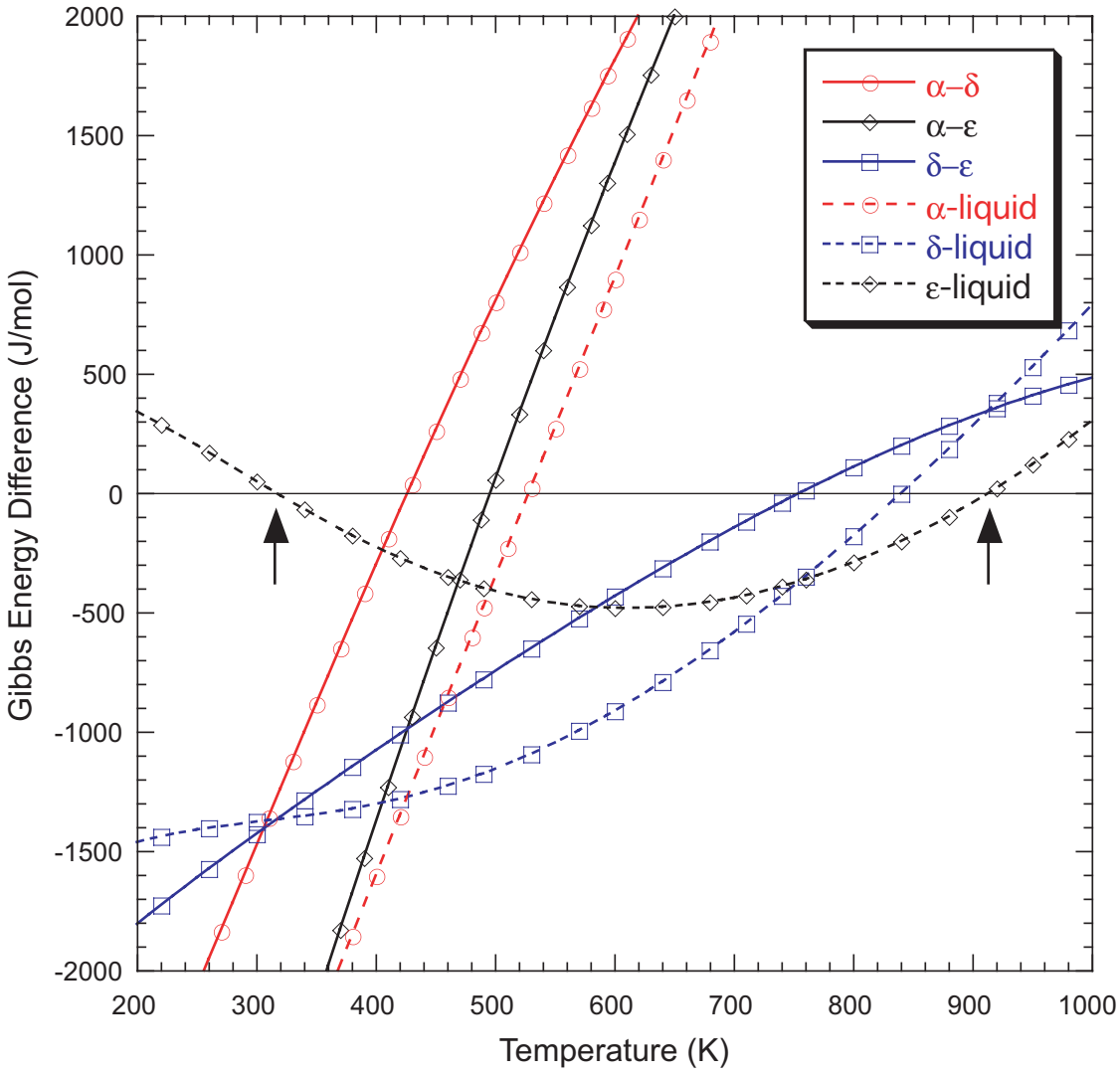

FIG. 8. Turchi *et al.*

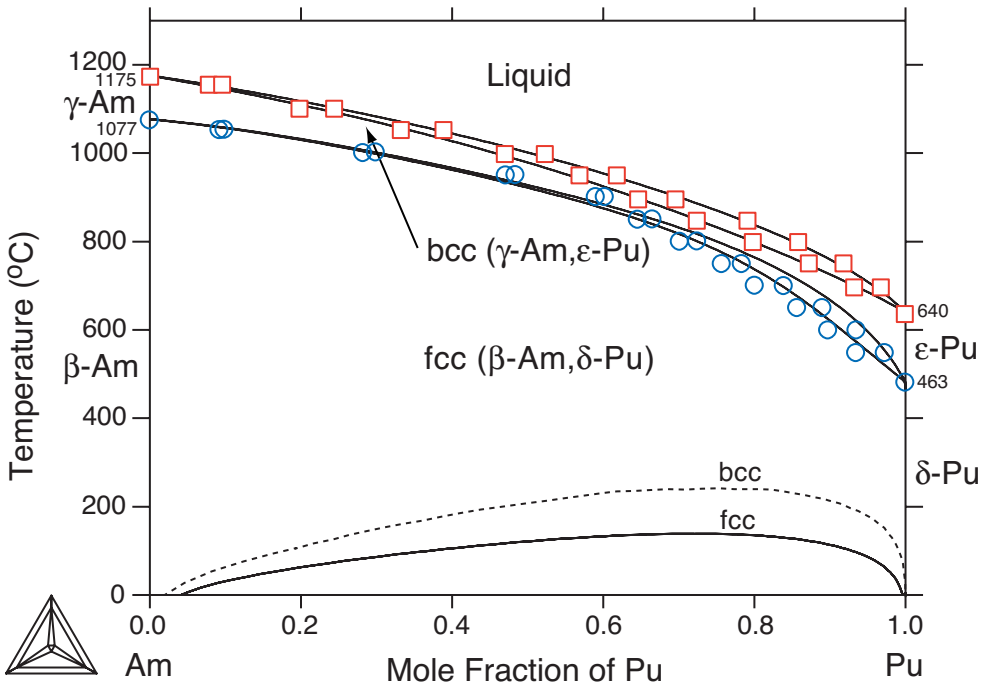

FIG. 9. Turchi *et al.*

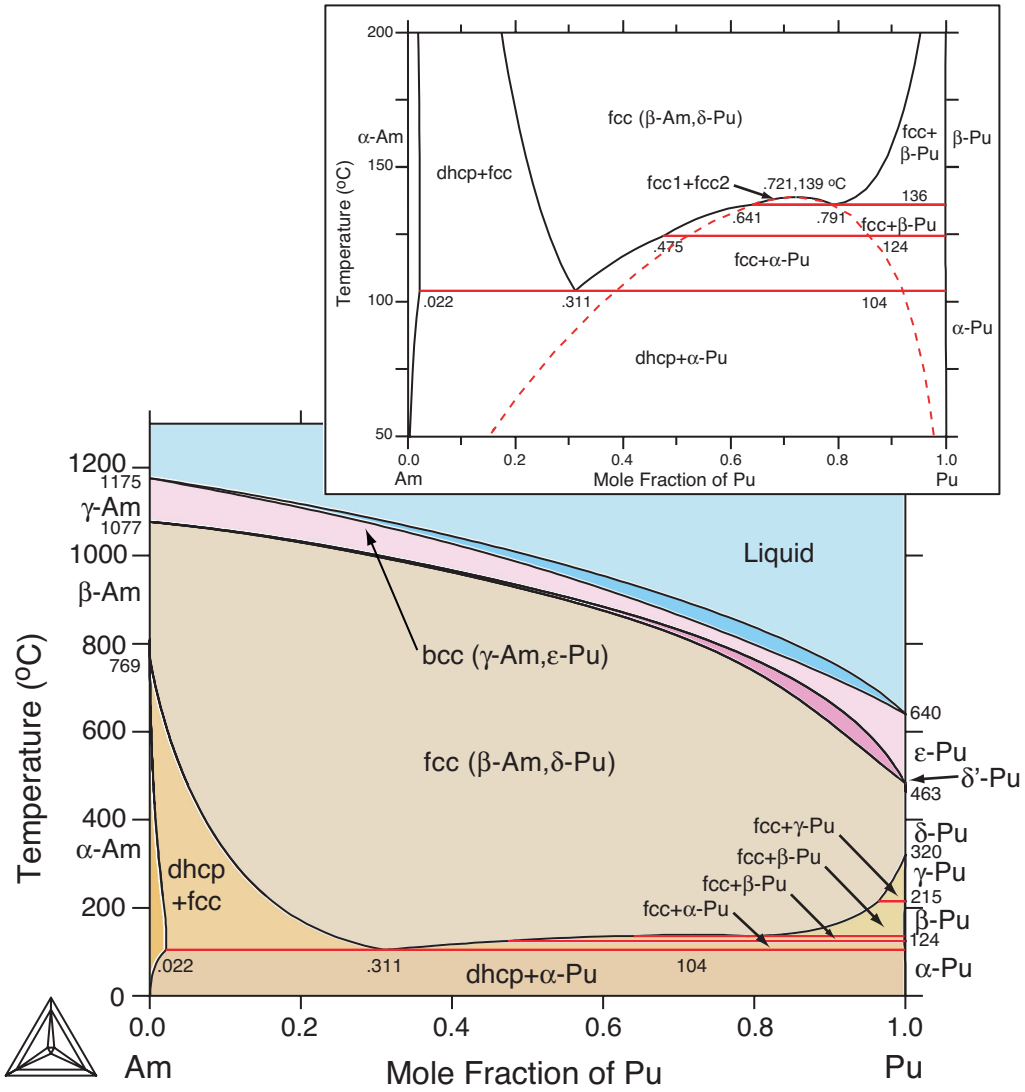

FIG. 10. Turchi *et al.*

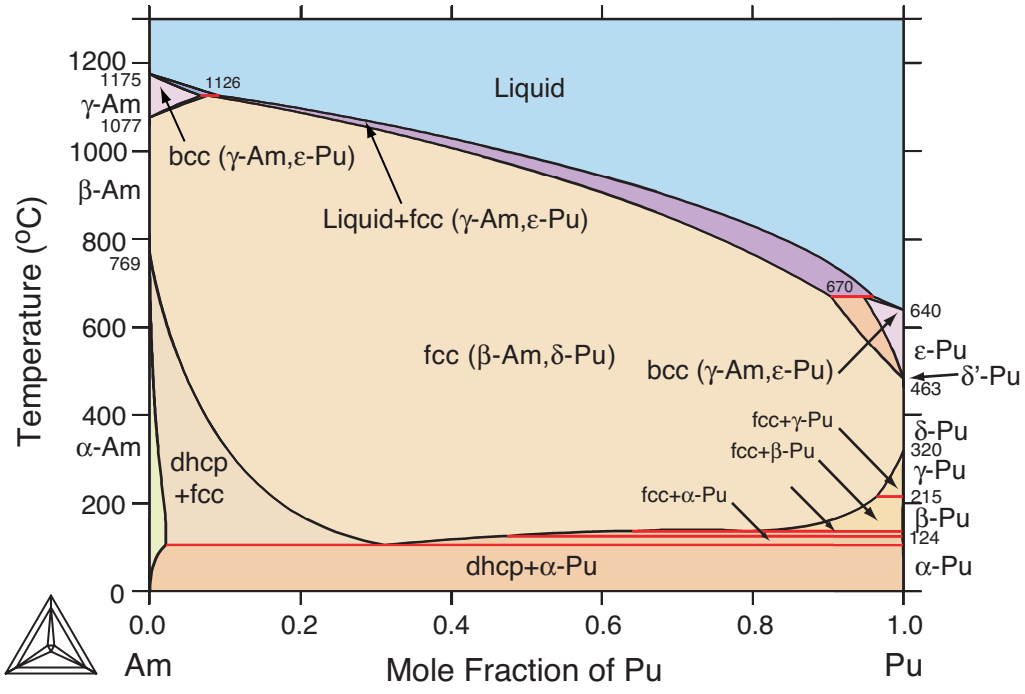

FIG. 11. Turchi *et al.*

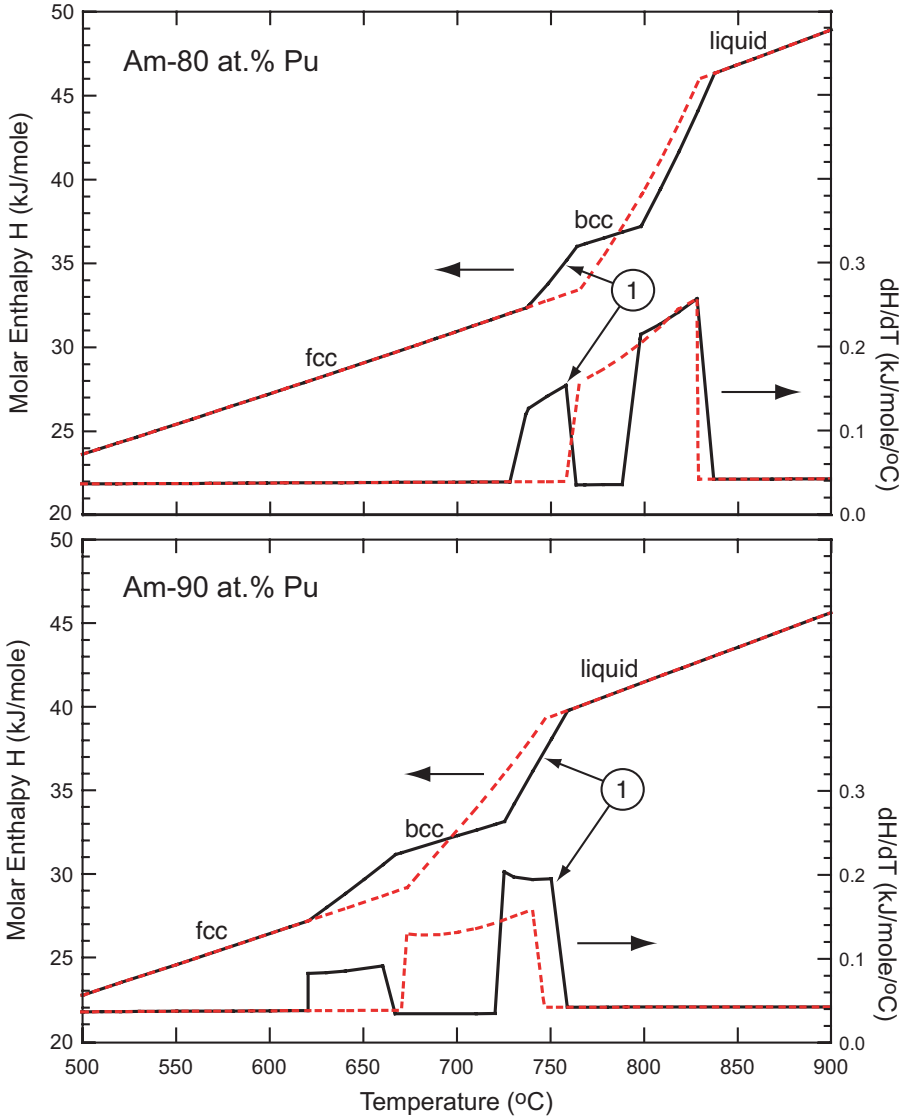

FIG. 12. Turchi *et al.*